Influence of Heavy Fermion Ytterbium Substitution on the Electronic and Crystal Properties of the Frustrated Magnet $CuFeO_2$ Oxide

OSMAN MURAT OZKENDIR

The influence of heavy fermion Ytterbium substitution was investigated on the crystal, electronic, and magnetic properties of $CuFeO_2$ with the general formula $Yb_xCu_{1-x}FeO_2$. The results of the crystal structure study revealed polycrystalline formations in the sample. The electronic and magnetic properties of the samples were studied using X-ray absorption spectroscopy (XAS) and X-ray magnetic circular dichroism (XMCD) techniques. Both XAS and XMCD revealed that the substituted Yb atoms govern the entire phenomena with their narrow 4*f* levels by forming broader molecular bonds with the 3*d* levels of the transition metals. Owing to the prominent changes caused by the activity of the 4*f* electrons in the crystal structures, Yb atoms were determined to be the main "role player" in the phase transitions. XMCD measurements were performed at room temperature 300 K (27 °C) to determine the magnetic properties of the samples and, except for $CuFeO_2$ ($x = 0.0$), the samples were observed to be ordered magnetically (mainly ferrimagnetic) in the bulk.

DOI: 10.1007/s11661-017-4308-2

I. INTRODUCTION

X-RAY absorption spectroscopy (XAS) is a powerful technique that probes electronic and bonding properties of elements. The strength of the technique attracts many scientists' attention who would like to find out necessary tools for their researches. X-ray absorption fine structure spectroscopy (XAFS) technique provides more detailed data with its two spectral parts than other techniques. A collected XAFS spectra can be processed in two parts; low photon energy part of the interested spectra which is called as the XANES (X-ray Absorption Near-Edge Spectroscopy) and beyond that part the second regime EXAFS (Extended-XAFS) region lies. The XANES region/part can provide fruitful information about the source atom's environment, *i.e.*, the bonding with the neighboring atoms, electronic structure of the interested atom in the materials and support the determination of local atomic arrangements. The data from the EXAFS region can yield precious information about the crystal structure of any material disregarding its crystallinity (crystalline or non-crystalline).

The electronic and magnetic properties of iron oxides render them a popular class of transition metal oxides. Iron-based technologies have attracted significant interest from researchers for electronic and optoelectronic devices, mineralogy, magnetic materials, batteries, semiconductor materials, *etc.*[1–5] The high electronic interplay in the molecular structure of iron and its oxides reveals exciting physical phenomena. Therefore, new studies based on the strong electron correlations in transition metals are supported by the 4*f* group elements, *i.e.*, rare earths (RE), and researches with high impact on characteristics of these materials were reported in several papers.[6–8]

In a material containing *d–f* levels, the *d* shells of the transition metals are the main playground for strong electronic interactions with the outer shell electrons of the neighboring atoms. Due to the presence of densely localized electrons at the narrow *f*-energy bands, the interplay between *d–f* systems attracts huge attention due to the possibility to yield rich scientific results for technology.[9]

In this study, crystal, electronic, and magnetic properties of $CuFeO_2$ were investigated to determine the influence of heavy fermion Ytterbium substitution (with a decrease in Cu atomic concentration) with the general formula $Yb_xCu_{1-x}FeO_2$. Delafossite $CuFeO_2$ is a member of low-dimensional transition metal oxides (TMO) with a geometrically frustrated magnetic structure [T_N = 11 K and 14 K (−262 °C and −259 °C)] and forms in Rhombohedral "R-3m" crystal geometry with slightly distorted hexagonal layers.[2–4] Due to the

OSMAN MURAT OZKENDIR is with Mersin University, Tarsus Faculty of Technology, Energy Systems Engineering, 33400, Tarsus, Turkey. Contact e-mail: ozkendir@gmail.com
Manuscript submitted November 28, 2016.
Article published online September 1, 2017

change in cation valence bands, the crystal structure is highly affected by the oxygen non-stoichiometry.[2] The bonding between Fe and Cu atoms is governed by their 3*d* levels with fivefold degeneracy, and it brings the atoms to each other closer than usual and builds the $CuFeO_2$ oxide crystal. Occupied *d* shells of both iron and copper can provide rich quantum symmetry in electronic interactions and supports interesting physical phenomena.[10–13]

II. EXPERIMENTAL

Samples with the general formula $Yb_xCu_{1-x}FeO_2$ (the values of x are; 0.0, 0.2, 0.4, 0.8, and 1.0.) were fabricated using the solid-state reaction method, which is one of the most popular methods for the preparation of bulk materials. These samples were synthesized from the stoichiometric mixtures of Yb_2O_3, Cu_2O, and α-Fe_2O_3 powder compounds with high purity as the starting materials (>99.99 pct Alfa-Aesar chemicals). In order to obtain fine powders for the desired materials, mixed materials were milled in ethanol using a magnetic stirrer at room temperature 300 K (27 °C) for 12 hours. In the second step, the samples were annealed up to 523 K (250 °C) for 6 hours and dried in air. Then, samples were milled in ethanol at room temperature for 24 hours and dried in air.

III. MATERIALS AND METHOD

The crystal structure properties of the prepared Yb-doped $CuFeO_2$ samples were studied using X-ray diffraction (XRD) patterns taken at the Advanced Materials research laboratory of Mersin University (Mersin, Turkey) (MEITAM) with Rigaku Smartlab model. XRD patterns were used to determine the crystal structure properties of the samples and also to support the X-ray absorption spectroscopy (XAS) data for further analysis. XRD patterns of the samples are shown in Figure 1, to illustrate the changes in the crystal structure. XRD patterns of the samples have multiple peaks that highlight the polycrystalline property of the samples.

To support the crystal structure analysis, morphological properties of the samples were estimated *via* their average crystallite sizes by using the most powerful reflection from the taken XRD patterns *via* Scherrer formula[11] which is given as

$$A = K\lambda/(\beta \text{ Cos } \theta). \quad [1]$$

In the formula, A is the average crystallite size; λ is the wavelength of the used X-ray beam (0.154056 nm); K is the Scherrer constant (0.94); θ is the Bragg angle, and β is the full width half maximum (FWHM) of the diffraction pattern. The estimated average crystallite sizes of the $Yb_xCu_{1-x}FeO_2$ substituted materials are given in Table I with other crystal analysis results. The crystallite sizes of the studied samples were determined

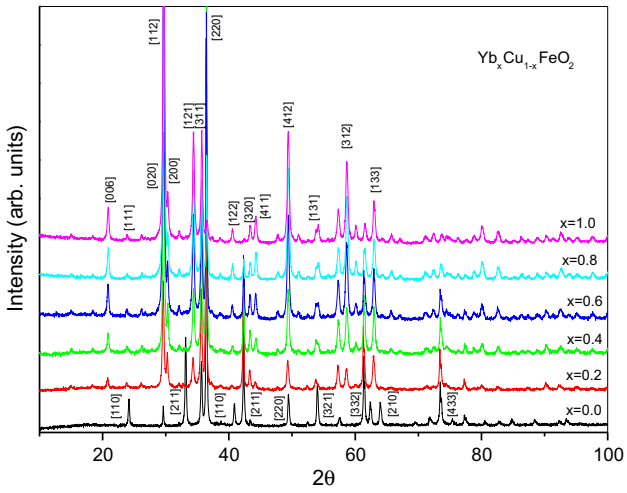

Fig. 1—Comparison of the XRD patterns of the $Yb_xCu_{1-x}FeO_2$ samples.

to be between 16 and 49 nm and a meaningful decrease in the size with the increase in the Yb doping amount was observed. Morphological results were used to enlight and support the study on the crystal structure properties of the samples. Crystal structure analysis was performed by using MAUD software which has the name from the capitals of Material Analysis Using Diffraction (MAUD) patterns. It is a diffraction/reflectivity analysis code, mainly based on the Rietveld method.[12]

According to the analysis results obtained from the XRD patterns, samples were observed to be polycrystalline in structure (not including the sample for $x = 0.2$, which is determined in one type of crystal structure). In the XRD patterns, the reflections of the intensities are defined and shown in Figure 1 for the samples $CuFeO_2$ and $YbFe_2O_4$ as a guide for the readers. In Figure 1, with the increase in Yb substitutions, Yb reflections appeared beyond $x = 0.0$ samples and became more strong while Cu-centered reflections have meaningful decay.

Slight shifts were observed at some strong peak intensities in this figure as a result of the changes in site symmetries. The analysis on the contribution of Yb to the properties of $CuFeO_2$ material are presented with in the substitution steps ($x = 0.2$, 0.4, 0.6, and 0.8).

A. *Unsubmitted $Yb_xCu_{1-x}FeO_2$ ($x = 0.0$ and 1.0) Samples*

In Figure 1, a comparison of the XRD patterns of the samples is shown and the reflections are highlighted on the peaks as a guide for other samples. According to MAUD analysis, the sample $x = 0.0$ was observed to form in two similar geometries: $CuFeO_2$ and α-Fe_2O_3. The highest reflection peak intensity of the sample was determined from the [110] plane of $CuFeO_2$ lattices. Moreover, reflections of the hematite (α-Fe_2O_3) structure were also observed as the secondary formation in the polycrystalline sample with weaker peak intensities,

Table I. The Crystal Structure Analysis Results of Yb-Doped $CuFeO_2$ Samples

Substitution ($Yb_xCu_{1-x}FeO_2$)	Crystal	α	β	γ	a	b	c	Geometry	SG	Percent	Average Crystallite Size (nm)
$X = 0$	$CuFeO_2$	33.54	33.54	33.54	5.237	5.237	5.237	trigonal	R-3m:R	80	43.7
	Fe_2O_3	55.23	55.23	55.23	5.441	5.441	5.441	trigonal	R-3m:R	20	
$X = 0.2$	$YbCu_3\ Fe_4O_{12}$	90	90	90	10.056	10.056	10.056	cubic	Pn-3	100	49.09
$X = 0.4$	$YbCu_{0.4}Fe_{1.6}$	90	90	90	7.094	7.094	7.094	cubic	Fd-3m:1b	63	39.65
	$YbFeO_3$	90	90	90	4.137	5.530	6.026	orthorhombic	Pbnm:cab	37	
$X = 0.6$	$YbCu_3\ Fe_4O_{12}$	90	90	90	7.399	7.399	7.399	cubic	Im-3	39	16.09
	$YbFeO_3$	90	90	90	6.041	3.650	8.550	orthorhombic	Pbnm:cab	61	
$X = 0.8$	$CuFe_2O_4$	90	90	90	8.353	8.353	8.353	cubic	Fd-3m:2	28	27.9
	$YbFe_2O_4$	27.166	27.166	27.166	3.692	3.692	3.692	trigonal	R-3m:H	28	
	$YbCu_3Fe_4O_{12}$	90	90	90	7.386	7.386	7.386	cubic	Im-3	44	
$X = 1.0$	$YbFeO_3$	90	90	90	5.233	5.557	7.570	orthorhombic	Pbnm	09	26.77
	$YbFe_2O_4$	90	90	120	6.091	6.091	30.036	trigonal	R-3m:H	91	

and the concentration is lower in the bulk. The results of the MAUD analysis revealed that 80 pct of the bulk was formed with the $CuFeO_2$ structure, whereas the remaining 20 pct was formed with the α-Fe_2O_3 structure (given in Table I).

According to the crystal structure analysis; $CuFeO_2$ was determined as the main crystal structure in the sample with $x = 0.0$ which has trigonal crystal geometry with a space group of *R-3m:R* and it belongs to the mineral group of "Delafossite" with general formula of ABO_2. The lattice parameters of the structure were determined as follows: $a = 5.237$ Å and $\alpha = \beta = \gamma = 33.54$ deg. The delafossite $CuFeO_2$ is a member of low-dimensional transition metal oxide (TMO) with its geometrically frustrated magnetic properties and forms in rhombohedral *R-3m* crystal geometry with slightly distorted hexagonal layers.[2–4] Owing to the change in cation valence bands, the crystal structure is highly affected by the oxygen non-stoichiometry.[2] The rest of the sample structure (20 pct) was determined to be the parent α-Fe_2O_3 crystal structure with trigonal geometry and *R-3m:R* space group. Hematite is one of the parent oxide for this material and popular as one of the most studied members of iron oxides with antiferromagnetic ordering at room temperatures [Néel temperature $T_N = 950$ K (677 °C)].

The delafossite $CuFeO_2$ material is a popular field in recent researches because of peculiarities revealing interesting electronic and magnetic properties due to geometrically frustrated structure. To probe these properties of the samples, XAS study is a good choice and it can provide us useful informations about the electronic mechanisms and its related outcomes when a different material doped in the bulk.

The study of the electronic and magnetic structures of the $Yb_xCu_{1-x}FeO_2$ materials was performed using XAS data on the Fe $L_{3,2}$ and O K-edges. XAS data were collected at I1011 beamline of MAX-Lab Synchrotron laboratory which is located in Lund University campus area in Lund, Sweden. The beamline I1011 delivers the light from the ring MAX-II that uses an elliptically polarizing undulator and providing soft X-ray with a variable polarization state.[13] Fe $L_{3,2}$-edge and O K-edge measurements were performed at ultra high vacuum (UHV) conditions (approximately 10^{-10} Torr) with polarized light. The data were recorded with a total electron yield (TEY) mode by detecting a drain current from the sample and the energy resolution was set to 0.1 eV.

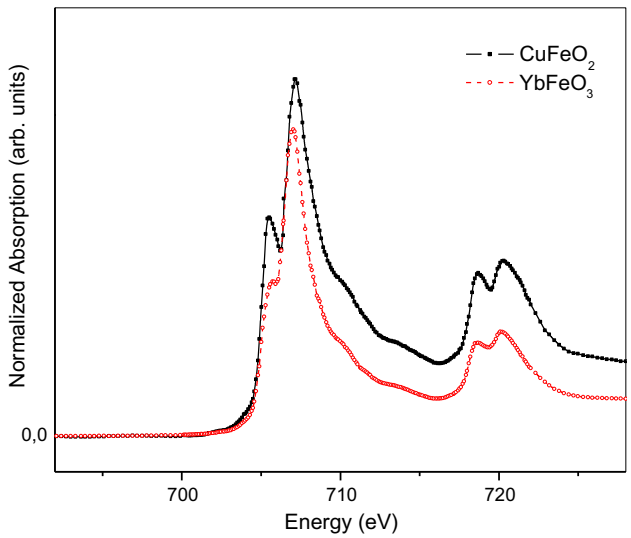

Fig. 2—Compared spectra of Fe $L_{3,2}$ edge XANES spectra for the samples $x = 0.0$ and $x = 1.0$.

In Figure 2, Fe $L_{3,2}$ XAS spectra of the samples for $x = 0.0$ and 1.0 are shown for comparison. The sample spectra are consistent in terms of peak positions and edge structures, which confirms that Fe atoms preserve their ionization as Fe^{3+} in the structures. Moreover, the sample spectra have two peaks confirming mainly two different crystal structures in the samples with low (α-Fe_2O_3 and $YbFeO_3$) and high concentrations ($CuFeO_2$ and $YbFe_2O_4$). The separated L_3 and L_2-edge spectra of the 3*d* metals are result of strong spin-orbit coupling between 2*p* core holes and 3*d* final states. Due to the strong coupling, crystal field splits the energies of the states into two levels that are given as separate L_3 and L_2 peaks. L_3-edge absorption peak is a result of the transitions of $2p_{3/2}$ electrons, while the L_2 edge

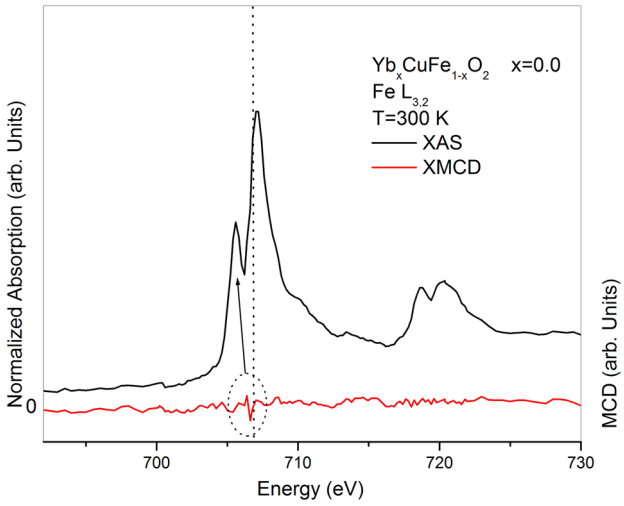

(a)

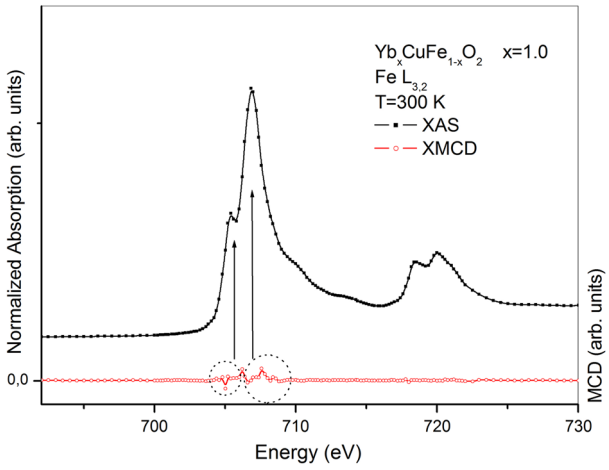

(b)

Fig. 3—(*a*) Fe $L_{3,2}$ edge XANES spectra of the sample for $x = 0.0$ and XMCD data at the room temperature. (*b*) Fe $L_{3,2}$ edge XANES spectra of the sample for $x = 1.0$ and XMCD data at the room temperature.

absorption peak corresponds to $2p_{1/2}$ core electrons' transitions to unoccupied 3*d* final states.[1–4,14]

For the sample with $x = 0.0$, Fe L_3-edge absorption spectra began to rise at 703 eV and exhibited two peaks on the main edge, with a weak edge at 705.5 eV and a strong edge at 707.1 eV. Two peak feature of the L_3-edge spectra is also presented at the L_2-edge spectra at 718.8 and 720.3 eV, respectively. Moreover, a weak post-edge structure was observed at 710.3 eV in both the spectra, but more intense for $x = 0.0$. The fivefold degeneracy of the 3*d* metals (Fe and Cu) supports low energy levels as t_{2g} (xy, yz, xz) for the pre-edge and the main edge levels. However, the post edge is a result of weakly bonded metals through the high energy e_g (x^2–y^2, $3z^2$–r^2) levels. Moreover, the peaks on the edges are a result of two different site symmetry occurrences in the sample where the metals possesses different ionizations. The weak edge structure at the lower energy part of the L_3-edge spectra for $x = 0.0$ is due to the presence of α-Fe_2O_3 (hematite) structure in the bulk. Crystal geometries in the sample for $x = 0.0$ were determined

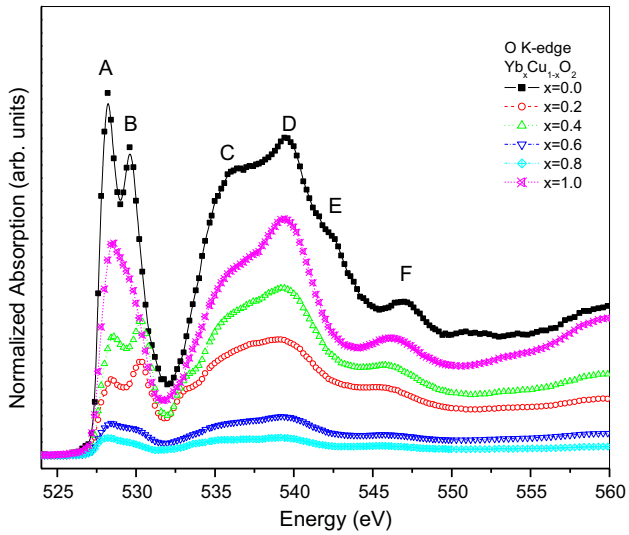

Fig. 4—Comparison of the Oxygen K-edge XANES spectra of the samples.

as the same (trigonal) but with different lattice parameters (distance and angle). The ratios of the spectral area values of the peaks for $x = 0.0$ and $x = 1.0$ were calculated as 3.97 [80 pct $CuFeO_2$ (strong peak) and 20 pct α-Fe_2O_3 (weak peak)] and 8.438 (91 pct YbFe2O4 [strong peak) and 09 pct $YbFeO_3$ (weak peak)]. The spectral area calculations confirmed the crystal structure ratios in the bulk as given in Table I.

Further, 91 pct of the sample bulk with $x = 1.0$ was observed to be of $YbFe_2O_4$ structure with trigonal geometry (*R-3m* space group), whereas 9 pct was observed to be of orthorhombic $YbFeO_3$ structure with the *Pbnm* space group. $YbFe_2O_4$ is a member of isostructural materials group with general formula "RFe_2O_4" and has been studied by scientists due its both magnetic and electronic properties as a well-known "spinel."[10,15] The electrical properties [ferroelectric below approximately 330 K (57 °C)] and antiferromagnetic ordering with Néel temperature (T_N) of 230 K to 250 K (−43 °C to −23 °C) were reported previously as a milestone in the studies of $YbFe_2O_4$ material.[15–17]

The crystal structure of 9 pct of the sample that was observed to be of $YbFeO_3$ structure was also studied intensively[6,18] and is a member of ABO_3 oxides group with its orthorhombic perovskite crystal structure.[18] The popularity of the material arises from its magnetic and ferroelectric properties with a high applicability to technology. Both hematite and $YbFeO_3$ are treated like an impurity in the samples and they have an influence in the crystal structure and especially in the magnetic properties of their neighboring blocks of $CuFeO_2$ and $YbFe_2O_4$.

In Figures 3(a) and (b), the magnetic orientation data of the samples with $x = 0.0$ and 1.0 are shown separately with their absorption spectra. The data for magnetic orientations of the samples were collected by X-ray magnetic circular dichroism (XMCD) technique at MAX-Lab BL-I1011. In Figure 3(a), the magnetic data for the hematite part in the XAS spectra are shown

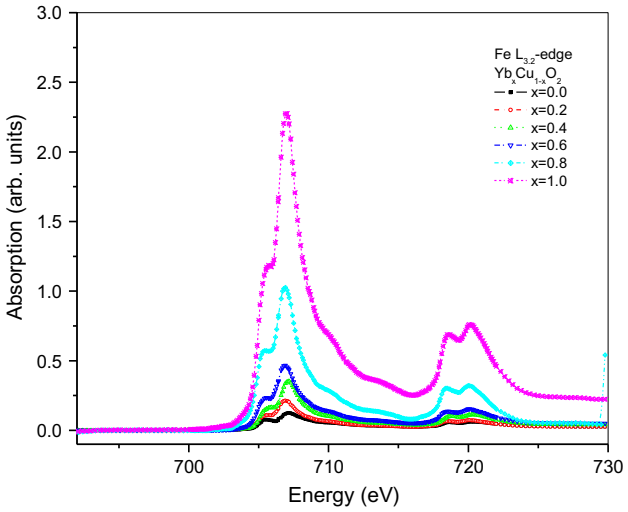

Fig. 5—Comparison of the Fe $L_{3,2}$-edge XANES spectra of the samples.

with a hollow dotted circle. Antisymmetric peaks with almost the same amounts of positive and negative values reveal the antiferromagnetic (AFM) ordering at room temperature for hematite regions. However, for the $CuFeO_2$ regions, no peak highlighting magnetic ordering was observed, which means thar $CuFeO_2$ regions have paramagnetic behaviors at room temperatures (RT) as reported previously.[2–4]

In Figure 3(b), X-ray magnetic circular dichroism (XMCD) data for the sample with $x = 1.0$ are shown along with its absorption (XAS) data. The magnetic data of the $YbFeO_3$ region of the magnetic spectra are confined with a hollow dotted circle, similar to the hematite region in Figure 3(a). As stated above, it is clearly visible from the figure that $YbFeO_3$ blocks possess a ferrimagnetic ordering at room temperature with a Néel temperature of approximately 630 K (357 °C) as reported elsewhere.[19] The strong peak in the figure is attributed to the $YbFe_2O_4$ material and it was reported to show paramagnetic ordering at RT and AFM ordering below 250 K (−23 °C).[15–17] However, in the figure, the magnetic spectral parts of the $YbFe_2O_4$ material show also weak ferrimagnetic features like $YbFeO_3$ materials. Interestingly, despite the lower concentration of $YbFeO_3$ materials, it appears that the influence of ferrimagnetically ordered $YbFeO_3$ blocks forced "spinel" $YbFe_2O_4$ blocks to order ferrimagnetically. In spinels, magnetic ordering can be explained by the mean field theory: the theory considers the exchange interactions between cations, *i.e.*, oxygen atoms in the structure, and the magnetic ordering are related to oxygen-mediated superexchange interactions between magnetic ions.[20] Superexchange is an electronic activity hopping between magnetic cations (Fe) and anions (O).

In the samples, oxygen atoms are treated as an agent to collect data from the atomic environment. Because, oxygen atoms sit between the 3*d* and 4*f* elements. Oxygen 2*p* levels are unoccupied and can overlap easily with the outer shell electrons of the metal atoms (Cu, Fe) due to its *p*-symmetry. However, for the *f*-elements, interaction with *p* electrons is forbidden due to dipole selection rules. To see the influence of *p–f* interplay is difficult on the Fe L-edge, because *p* or *f* interplay with the *d*-levels obey dipole selection rules, but oxygen K-edge spectra can give us better tools to analyze. Oxygen K-edge absorption spectra are the result of excited 1*s* electrons' transition to valence 2*p* levels. So, in case of any electronic interactions between *s* and *p–d–f*, a particular pre-edge structure should appear on the oxygen K-edge spectra and highlight forbidden transition between O-Fe/Cu/Yb atoms. In Figure 4, a comparison of the O K-edge absorption spectra of all the studied samples is shown. All the samples (except the sample with $x = 1.0$) have a strong pre-edge structure with two peaks, which highlight the low energy and high energy 3*d* levels of both Fe and Cu atoms. The pre-edge region for the sample with $x = 1.0$ has only one peak reflecting a narrower pre-edge feature owing to the contribution of *f*-electrons.

Oxygen has high electronegativity and it can interact with almost all neighboring atoms *via* electron coupling as a result of hybridization between O 2*p* and 3*d* levels of the transition metals. Bonding mechanisms that build a molecular band can keep them in the core of interplays and make them sensitive to the local bonding and symmetry. The splitted pre-edge structure (except sample with $x = 1.0$) has the strongest peak at 528.4 eV (assigned as "A") and the second peak has lower intensity at 529.45 eV (assigned as "B"). The intensity of the pre-edge peaks reflects the power of the strong coupling between the 2*p*–3*d* outer shell electrons of the neighboring Fe(Cu)-O atoms. The first peak is related to the lower energy levels in the hybrid *p–d* molecular bands. The main route for an excited 1*s* electron of the oxygen atom is the unoccupied *p*-levels, which provide a large main absorption edge. However, with the close energies and short distances of the valence levels of the neighboring atoms can support them to couple when wave vectors of their electrons' overlap and they can build hybridized molecular bonds with lower energy but with rich quantum symmetries. The pre-edge feature is also the result of crystal irregularities in the sample where an interested atom is involved in the structure. The main absorption peak of the O K-edge is the result of transitions of excited 1s electrons to unoccupied valence 2*p* levels. The high intensity and broad structure of the main edge highlight a rich final state with an abundance of unoccupied states and larger molecular band formation. There are four separate peaks on the main edge, which are denoted as "C," "D," "E," and "F" at 536.1, 539.35, 542.3, and 546.9 eV, respectively. Every peak appears as a result of hybridization with the 4*p* levels of the neighboring atoms, *i.e.*, Fe and Cu.

B. *Substituted $Yb_xCu_{1-x}FeO_2$ ($x = 0.2, 0.4, 0.6,$ and 0.8) Samples*

In this part of the study, influence of heavy fermion "Yb" substitution in the samples was investigated. In Figure 5, Fe $L_{3,2}$-edge spectra of all the Yb-doped and undoped samples are shown for comparison. In the spectra, the samples with $x = 1.0$ and $x = 0.0$ have the

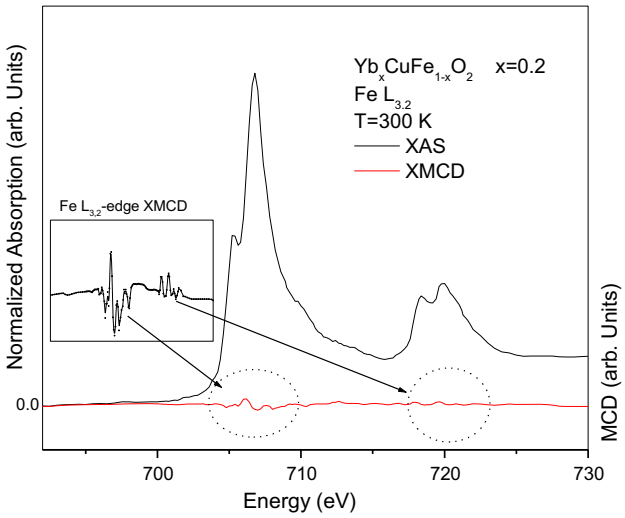

Fig. 6—Fe $L_{3,2}$ edge XANES spectra of the sample for $x = 0.2$ and XMCD data at the room temperature. Inset: XMCD spectra for Fe $L_{3,2}$-edge spectra for the sample $x = 0.2$ in its scale.

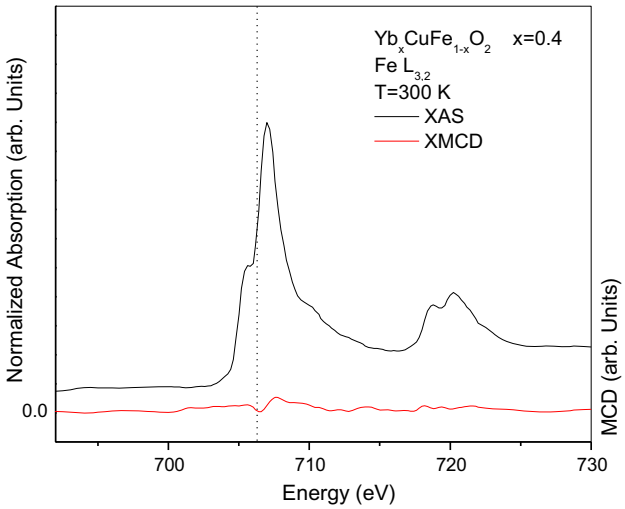

Fig. 7—Fe $L_{3,2}$ edge XANES spectra of the sample for $x = 0.4$ and XMCD data at the room temperature.

highest and the lowest absorption intensities, respectively. The peak intensity decreases consistently with the increase in Cu concentration. The reduction of *d*-level intensity with the increase in Cu in the Fe environment highlights Fe *d*-level suppression by the neighboring Cu 4*p* levels *via* hybridization. Owing to the presence of *p*-symmetry in the *d* final states, these levels are "forbidden" according to the quantum selection rules.

XRD pattern of the samples, in Figure 1, has multiple peaks, which confirms polycrystalline property in the samples. By using the marked reflections on the patterns, for the samples with $x = 0.0$ and 1.0 as references, lattices with Cu and Yb peaks can easily be recognized with a decrease for Cu-containing structures and increase with the Yb-containing lattice reflections with the order of x. According to the analysis of crystal structure, the sample with $x = 0.2$ was formed mainly in one type of crystal structure, $YbCu_3Fe_4O_{12}$, with cubic geometry ($a = 10.056$ Å) and the "Pn-3" space group. The structure has been reported in literature with the general formula "$\mathbf{A}Cu_3Fe_4O_{12}$" general formula where "A" denotes the A^{3+} cation of Lanthanides, Ca, Sr, and Ba. The crystal structure is reported as a member of perovskite-type transition metal oxides with properties such as, superconductivity, ferromagnetism, ferroelectricity, and magnetotransport.[21] The general formula where Lanthanides sit at *A*, was reported mainly as showing AFM ordering at room temperature. Although the sample was determined to possess one type of crystal structure, the multiple peak property of the XRD pattern reflects structural distortions originating from the size differences of heavy fermion and other members.[21]

In Figure 6, Fe $L_{3,2}$-edge XAS spectra for the sample with $x = 0.2$ are shown along with its XMCD data. Fe L_3-edge absorption spectra begin to rise at 703 eV and have two peak with a weak edge at 705.43 eV and the main edge at 706.8 eV. Two peak feature of L_3-edge spectra is also presented at the L_2-edge spectra at 718.4 and 720.04 eV, respectively. Besides, a weak post-edge structure is also observed at 710.1 eV, like the samples with $x = 0.0$ and 1.0. As reported for the "$\mathbf{A}Cu_3Fe_4O_{12}$" general formula Lanthanides, Yb^{3+}-substituted sample is also determined to show weak ferrimagnetic ordering at room temperature. Owing to the weak intensity of the circular dichroism data according to the absorption data, the XMCD data are shown in the inset of Figure 6 with a low intensity scale.

The sample with $x = 0.4$ also has multiple peaks in its XRD spectrum. According to the analysis (Table I), two different crystal structures were observed in the bulk.[22] The $YbCu_{0.4}Fe_{1.6}$ structure accounted for 63 pct of the sample, and has cubic geometry and the *Fd-3m* space group (lattice parameter $a = 7.094$ Å). This crystal structure was first studied by Chau *et al.* for the general formula $Er(Fe_xCu_{1-x})_2$ (where $x = 1.0$, 0.95, 0.9, 0.85, and 0.8).[23] In their study, they reported the series as showing ferrimagnetic ordering up to 500 K (227 °C) and possessing important features such as a high ordering temperature T_c, spin reorientation, and a huge *RT* magnetostriction.

The rest of the sample (37 pct) observed to be formed of $YbFeO_3$ crystal structure. The crystal structure possesses orthorhombic geometry with the "Pbnm" space group and defined lattice parameters are, $a = 4.137$ Å, $b = 5.530$ Å, $c = 6.026$ Å. The $YbFeO_3$ crystal structure belongs to $ReFeO_3$-type oxides and, orthoferrites and is characterized by corner-linked FeO_6 octahedra.[18]

In Figure 7, the XAS spectra for the sample with $x = 0.4$ with two different crystal structures are shown along with the magnetic XMCD data. Fe L_3-edge absorption spectra began to rise at 703.1 eV and have two peaks with a weak edge at 705.7 eV, and the main edge at 707.1 eV. Two peaks of the L_3-edge spectra were also presented on the L_2-edge spectra at 718.8 and 720.3 eV. Also, a weak post-edge structure was observed at 710.3 eV at both spectra. All data are in symmetry with the sample for $x = 0.0$. The ratios of the spectral areas

of the Fe-sites in the XAS spectral data were estimated as 1.57 (*i.e.*, $A_{YbCu0.4Fe1.6}/A_{YbFeO3}$), which is consistent with the result of the crystal structure analysis.

According to Figure 5, where the XAS spectra of all the samples shown for comparison, the edge intensities and structure highlights suppressed the iron atoms with Yb heavy fermions *via* 5*d* levels. Further, 3*d* electrons may couple with 4*f*-levels and strong overlapping can result in hybridized molecular bands. However, lack of oxygen in the main interplay causes poor quantum symmetry with Yb atoms where *d*-electrons can not interact with the 5*d* levels of Yb due to dipole selection rules. Besides, a slight shift to the higher energy side of the L_3-edge by 0.2 eV is a result of non-oxidized Fe atoms in the $YbCu_{0.4}Fe_{1.6}$ crystal structure. The XMCD data are shown below the XAS spectra in Figure 7 and it shows ferromagnetic ordering at *RT* as stated in the study by Chau *et al*. The dotted line in the figure is presented as a guide for eyes.

For the sample with $x = 0.6$, the results of XRD analysis revealed two main crystal structures formed in the bulk. XRD pattern analysis showed that the sample mainly formed was the $YbFeO_3$ crystal structure (61 pct) similar to the sample with $x = 0.4$. The defined lattice parameters for the $YbFeO_3$ crystal structure are as follows: $a = 6.041$ Å, $b = 3.650$ Å, $c = 8.550$ Å. The rest of the sample was formed in a familiar crystal structure $YbCu_3Fe_4O_{12}$ with cubic geometry ($a = 7.399$ Å) but with a different space group *i.e.*, *Im-3* as compared to the structure in the sample with $x = 0.2$. The results revealed a fact that, in the samples, there is a different mechanism causing a change in space group symmetry and make the atomic orientations with strong electronic correlations. For a deeper analysis and to investigate the background information in the sample, we should focus on the XAS and XMCD data of the sample. In Figure 8, the XAS spectra of the sample with $x = 0.6$ are shown along with its XMCD data. Fe $L_{3,2}$-edge spectra also have a pre-edge below the main absorption edge at 705.13 eV, which is attributed to the transition of the $2p_{3/2}$ electrons of the iron atoms in the $YbCu_3Fe_4O_{12}$ crystal structure. The main edge has also a peak at 706.68 eV which is attributed to the excited $2p_{3/2}$ electrons in the $YbFeO_3$ structures. In this sample, a weak dished pre-edge feature appeared at 704.6 eV and it surprisingly indicates an *f*–*d* hybridization between Yb-Fe levels. This mechanism was confirmed by the O K-edge spectra shown in Figure 4, where oxygen absorption spectra have a strong decay due to 3*d*–4*f* hybridized molecular bands, and provide forbidden quantum symmetry both for 1*s* and 2*p* electrons. This pre-edge feature in the XAS spectra is the most prominent among all the samples and reveals the strong coupling between the outer shells of Yb and Fe (and possibly Cu). Such a mechanism can bring the Fe and Cu atoms closer to each other, and interplays between *d*–*d* interactions can occur more strongly than in the other samples. The *d*-*d* interactions can built metal bonding at the high energy e_g levels of the molecular band. In the L_3-edge spectra, post edge peak located at 710.1 eV confirms the strong coupling between Fe 3*d*-3*d* Cu electrons. Moreover, the L_2-edge has two main peaks similar to others, but the third peak beyond the main edge at 721.1 eV is stronger (*d*–*d* coupling).

In Figure 8, the XMCD spectra are presented below the XAS spectra. Both the edge features are shown by arrows with their dichroic signals confined in the dot circle. The XMCD spectra of this sample have more powerful signal and confirm the ferrimagnetic ordering of Fe blocks both in $YbFeO_3$ and AFM ordering in $YbCu_3Fe_4O_{12}$ crystal structures. The higher intensity also indicates the contributions of *f*-electrons to strong *d*–*d* interactions, which cause antiparallel ordering of both Fe-Fe and Fe-Cu blocks *via* hybridized *f*-level symmetry containing molecular bands.

The higher Yb substitution takes place in the sample with $x = 0.8$ and revealed the most interesting properties among others, where low amount of Cu atoms in the bulk is treated like an impurity. According to the analysis result, the sample has polycrystalline structure property with formed three different crystal structures. As in the previous samples, $YbCu_3Fe_4O_{12}$ crystal structure possesses the main portion with 44 pct in the bulk. The lattice parameters are determined in cubic geometry, *Im-3* space group, and the lattice distance is $a = 7.386$ Å. Rest of sample is formed in two familiar crystal structures with the same amounts. Defined parameters for the crystal structures were determined in trigonal $YbFe_2O_4$ crystal structure (with "R-3m:H" space group and $\alpha = \beta = \gamma = 27.166$ degs $a = b = c = 3.692$ Å) and cubic $CuFe_2O_4$ crystal structure (with *Fd-3m* space group and $a = b = c = 8.353$ Å). According to the Fe $L_{3,2}$-edge spectra comparison given in Figure 5, the spectra for the sample with $x = 0.8$ have the second highest peak reflecting the rich unoccupied *d*-levels as a final state for *p*-electrons to locate. This confirms *d*-rich molecular band formation *via* Fe 3*d* and Cu 3*d* interaction *via d*–*d* metal bonding. However, O K-edge has one of the weakest intensities among others and addressing *f*-level contribution on the molecular bands.

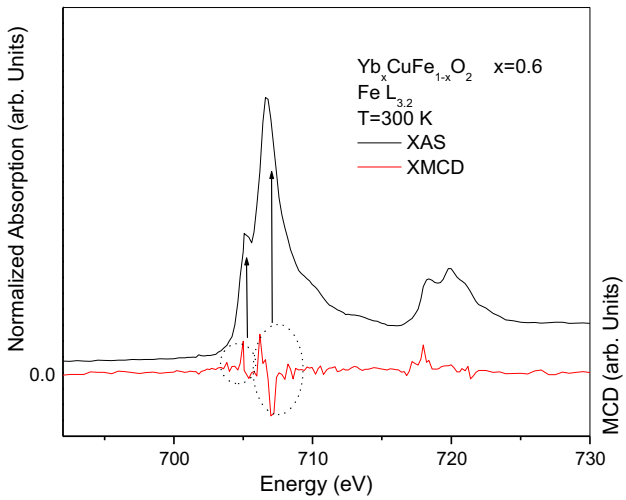

Fig. 8—Fe $L_{3,2}$ edge XANES spectra of the sample for $x = 0.6$ and XMCD data at the room temperature.

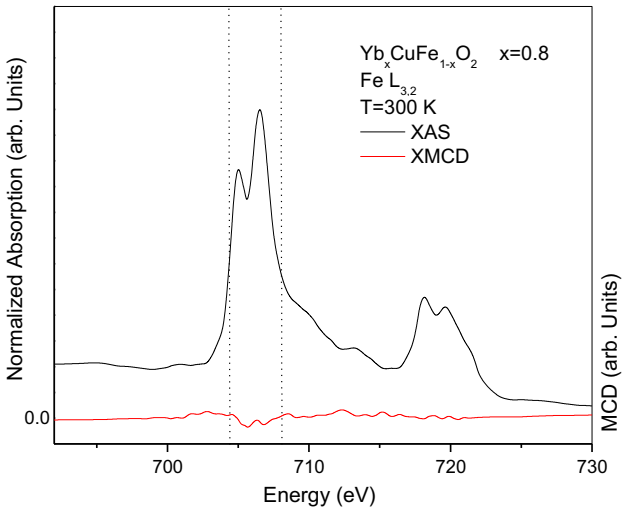

Fig. 9—Fe $L_{3,2}$ edge XANES spectra of the sample for $x = 0.8$ and XMCD data at the room temperature.

The Fe $L_{3,2}$-edge XAS spectra of the sample are given in Figure 9 and a weak pre-edge structure at 703.1 eV that emphasizes *f*-electrons contribution to the molecular band formations. The spectra also have two main edges; at the lower photon energy (705.04 eV) belongs to the crystal structure $YbFe_2O_4$ with trigonal geometry where Fe atoms exist as Fe^{2+} ionization in the sample. As a result of the different ionizations, the absorption intensity at the lower edge became sharper and split from the main edge. Like other samples, a post-edge feature presented at 710 eV highlights the *d–d* metal bonding between neighboring Fe-Cu atoms. The strength of the *d–d* bonding is a result of the weakness of bonding with oxygen in the sample among others. The influence of *d–d* metal bonding on the magnetic behaviors of atoms can be probed by the XMCD data, which is shown below the XAS spectra in Figure 9. The magnetic orientations show mostly antiferromagnetic or ferrimagnetic ordering of the polycrystalline materials. However, despite the polycrystalline structure with three different crystal formations in the bulk, the Fe blocks in the sample show ferromagnetic ordering, which can be expressed as a result of strong interplay between close neighbors outer shell electrons.

IV. CONCLUSION

In this study, the influence of the heavy fermion Ytterbium substitution in Cu coordination of the frustrated magnet delafossite $CuFeO_2$ samples on their crystal, electronic, and magnetic properties was investigated with the general formula $Yb_xCu_{1-x}FeO_2$. The samples were mainly observed to be polycrystalline materials and a significant decrease in the crystallite sizes was observed with the increase in the substituted heavy fermion Yb. XAS and XMCD techniques were used to probe the electronic and magnetic properties of the samples. Substituted Yb atoms were determined to govern the entire phenomena with their narrow 4*f*-levels by forming broader molecular bands with the 3*d* levels of the transition metals.

The parent oxide $CuFeO_2$ was reported to be antiferromagnetically ordered at low temperatures in literature by several papers. In this study, the magnetic properties of the samples were also tested at room temperature by using XMCD measurements. As a result of the study, all the samples, except $CuFeO_2$ domains, were observed to show magnetic ordering (mainly ferrimagnetic) at room temperatures. However, the sample with $x = 0.8$ was solely observed to show ferromagnetic ordering at room temperatures owing to the strong spin interplay between the different domains oriented along the iron blocks.

ACKNOWLEDGMENTS

The author would like to thank to Dr. Gunnar Ohrwall from MAX-lab. Beamline I1011 (Lund, Sweden). This study was supported financially by "2015-AP4-1153" project of Mersin University (Mersin, Turkiye). Additionally, the research leading to these results has received funding from the European Community's Seventh Framework Program (FP7/2007-2013) CALIPSO under Grant Agreement No 312284.

REFERENCES

1. P.S. Miedema and F.M.F. De Groot: *J. Electron Spectrosc. Relat. Phenom.*, 2013, vol. 187, pp. 32–48.
2. O.M. Ozkendir : *J. Electron. Mater.*, 2013, vol. 42 (6), pp. 1055–62.
3. K. Mori, M. Hachisu, T. Yamazaki, and Y. Ichiyanagi: *J. Appl. Phys.*, 2015, vol. 117, p. 17C756.
4. O.M. Ozkendir: *J. Metall. Mater. Trans. A*, 2016, vol. 47A, pp. 2906–13.
5. H. Takahashi, Y. Motegi, R. Tsuchigane, and M. Hasegawa: *J. Magn. Magn. Mater.*, 2004, vol. 217, pp. 272–76.
6. L.J. Downie, R.J. Goff, W. Kockelmann, S.D. Forder, J.E. Parker, F.D. Morrison, and P. Lightfoot: *J. Solid State Chem.*, 2012, vol. 190, pp. 52–60.
7. V. Krishnan, R.K. Selvan, C.O. Augustin, A. Gedanken, and H. Bertagnolli: *J. Phys. Chem.*, 2007, vol. C 111, pp. 16724–33.
8. I. Yamada: *J. Ceram. Soc. Jpn.*, 2014, vol. 122 (10), pp. 846–51.
9. C. Ruihua, C.N. Bora, P.A. Dowbcena, S. Stadler, and Y.U. Idzerda: *Appl. Phys. Lett.*, 2001, vol. 78 (4), p. 521.
10. K. Yoshi, M. Mizumaki, K. Matsumoto, S. Mori, N. Endo, H. Saitoh, D. Matsumura, T. Kambe, and N. Ikeda: *J. Phys.*, 2013, vol. 428, p. 012032.
11. H.O. Abd-Alkader and N.M. Dearz: *Int. J. Electrochem. Sci.*, 2013, vol. 8, pp. 8614–22.
12. L. Lutterotti and M. Bortolotti: *IUCr*, 2003, vol 1, p. 43.
13. I.A. Kowalik, G. Öhrwall, B.N. Jensen, R. Sankari, E. Wallen, U. Johansson, O. Karis, and D. Arvanitis: *J. Phys.*, 2010, vol. 211, p. 012030.
14. O.M. Ozkendir: *J. Optoelectron Adv. Mater. Rapid Commun.*, 2009, vol. 3, p. 586.
15. N. Ikeda, H. Ohsumi, K. Ohwada, K. Ishii, T. Inami, Y. Murakami, K. Kakurai, K. Yoshii, S. Mori, Y. Horibe, and H. Kito: *Nature*, 2005, vol. 436, p. 1136.
16. K. Yoshii, N. Ikeda, Y. Matsuo, Y. Horibe, and S. Mori: *Phys. Rev. B*, 2007, vol. 76, p. 024423.
17. K. Oka, M. Azuma, N. Hayashi, S. Muranaka, Y. Narumi, K. Kindo, S. Ayukawa, M. Kato, Y. Koike, Y. Shimakawa, and M. Takano: *J. Phys. Soc. Jpn.*, 2008, vol. 77, p. 064803.
18. Y.K. Jeong, J.-H. Lee, S.-J. Ahn, S.-W. Song, H.M. Jang, H. Choi, and J.F. Scott: *J. Am. Chem. Soc.*, 2012, vol. 134, pp. 1450–53.

19. H. Pinto, G. Shachar, and H. Shaked: *Solid State Commun*., 1970, vol. 8 (8), pp. 597–99.
20. M.A. Willard, Y. Nakamura, D.E. Laughlin, and M.E. McHenry: *J. Am. Ceram. Soc*., 1999, vol. 82 (12), pp. 3342–46.
21. I. Yamada: *J. Ceram. Soc. Jpn*., 2014, vol. 122 (10), pp. 846–51.
22. L. Lutterotti and M. Bortolotti: *IUCr*, 2003, vol. 1, pp. 43–50.
23. N.H. Chau, N.H. Dug, T.D. Hien, K. Krop, and J. Zukrowsk: *Phys. Status Solidi (A)*, 1989, vol. 114, pp. 361–67.